Myocardial T1 mapping using an Instantaneous Signal Loss Simulation modeling and a Bayesian Estimation Method

Timothé Boutelier, Habib Rebbah, Kevin Tse-Ve-Koon, Pierre Croisille, Magalie Viallon

IEEE Transactions on Medical Imaging

Myocardial T1 mapping using an Instantaneous Signal Loss Simulation modeling and a Bayesian Estimation Method

Journal:	*IEEE Transactions on Medical Imaging*
Manuscript ID	TMI-2021-0435
Manuscript Type:	Regular Paper
Date Submitted by the Author:	15-Mar-2021
Complete List of Authors:	Boutelier, Timothé; Olea Medical, Research and Innovation Rebbah, Habib; Olea Medical, Reasearch and Innovation Tse Ve Koon, Kevin; INSA Lyon; University Lyon 1;University of Lyon; CNRS UMR 5220; Inserm U1294, CREATIS CROISILLE, Pierre; INSA Lyon; University Lyon 1;University of Lyon; CNRS UMR 5220; Inserm U630, CREATIS Viallon, Magalie; INSA Lyon; University Lyon 1;University of Lyon; CNRS UMR 5220; Inserm U1294, CREATIS
Keywords:	Magnetic resonance imaging (MRI) < Imaging modalities, Heart < Object of interest, Probabilistic and statistical methods < General methodology, Quantification and estimation < General methodology

IEEE TRANSACTIONS ON MEDICAL IMAGING, VOL. XX, NO. XX, XXXX 2021

Myocardial T1 mapping using an Instantaneous Signal Loss Simulation modeling and a Bayesian Estimation Method

Timothé Boutelier,Habib Rebbah, Kevin Tse-Ve-Koon, Pierre Croisille, Magalie Viallon,

***Abstract*— The Instantaneous Signal Loss Simulation (InSiL) model is a promising alternative to the classical mono-exponential fitting of the Modified Look-Locker Inversion-recovery (MOLLI) sequence in cardiac T_1 mapping applications, which achieves better accuracy and is less sensitive to heart rate (HR) variations. Classical non-linear least squares (NLLS) estimation methods require some parameters of the model to be fixed *a priori* in order to give reliable T_1 estimations and avoid outliers. This introduces further bias in the estimation, reducing the advantages provided by the InSiL model. In this paper, a novel Bayesian estimation method using a hierarchical model is proposed to fit the parameters of the InSiL model. The hierarchical Bayesian modeling has a shrinkage effect that works as a regularizer for the estimated values, by pulling spurious estimated values toward the group-mean, hence reducing greatly the number of outliers. Simulations, physical phantoms, and *in-vivo* human cardiac data have been used to show that this approach estimates accurately all the InSiL parameters, and achieve high precision estimation of the T_1 compared to the classical MOLLI model and NLLS InSiL estimation.**

***Index Terms*— T1 mapping, MR relaxometry, myocardial imaging, Bayesian estimation, Shrinkage prior.**

I. Introduction

QUANTITATIVE T_1 mapping is a quantitative Magnetic Resonance Imaging (MRI) technique aiming at measuring the spin-lattice magnetization relaxation time (T_1) in tissue [1]. Being sensitive to the tissue microstructure, T_1 turns out to be an important biomarker used to characterize tissue, and differentiate between healthy and pathological regions of an organ. It has many important clinical applications, for neurodegenerative diseases characterization, myelin mapping, brain aging studies, liver fibrosis quantification, in oncology, and in Cardiac Magnetic Resonance (CMR) [2], [3].

T_1 mapping is widely used in CMR for pathologies where myocardial tissue remodeling is characteristic of the pathology. Native (non-contrast) T_1 is sensitive to fluid accumulation in the injured tissue, hence allowing the detection of the oedema via an increase of the T_1 [4], [5]. Because the injection of a paramagnetic contrast agent modifies the T_1 of a perfused tissue, post-injection T_1 mapping reveals differences of permeability properties between tissues, and allow to compute the extra-cellular volume (ECV) [6], [7]. This biomarker directly derived from T_1 mapping is a proxy for the detection and quantification of diffuse myocardial fibrosis [8].

Inversion Recovery spin echo (IR) is the "gold standard" sequence for measuring T_1 values, by sampling the longitudinal magnetization recovery with a conventional spin echo (SE) sequence at different inversion times (TI) after a $180°$ inversion pulse. Although robust, this sequence has a very long acquisition time, which prevents its application in clinical CMR. Fast and accurate sequences have been developed since then to allow for myocardial T_1 mapping in a single breath-old duration: inversion recovery based sequences like the modified Look-Locker inversion recovery (MOLLI) [9], saturation recovery based sequences like the SAturation-recovery single-SHot Acquisition (SASHA) [10], or hybrid sequences like the SAturation Pulse Prepared Heart rate independent Inversion-REcovery sequence (SAPPHIRE) [11].

Among them, the MOLLI sequence is the most commonly used in the clinical practice. However, it has some limitations due to bias induced by HR variation, T_1 and T_2 tissue properties, or imperfect inversion [3], [12]. The InSiL model [12] was introduced in an attempt to reduce those bias by modeling the complete evolution of the magnetization during the sequence. Imperfect inversion, read-out losses, and imperfect magnetization recovery are taken into account by the model, which showed promising results [12], [13]. However the model is ill-conditioned and NLLS optimization of the parameters yields spurious parameter estimation. To overcome this issue, [12] proposed to fix some parameter of the model like the inversion efficiency to an *a priori* constant value for all voxels, that would have been previously estimated with an independent method [14]. This approach efficiently stabilizes the estimation problem, and allows to propose realistic T_1 maps. Still, this approach may not be feasible in clinical practice since it requires a modified, longer, MOLLI sequence

This work was supported by the RHU MARVELOUS (ANR-16-RHUS-0009) of l'Université Claude Bernard Lyon 1 (UCBL), within the program "Investissements d'Avenir" operated by the French National Research Agency (ANR).

The authors would like to thank Michel Ovize, Thomas Bochaton, and Nathan Mewton, for sharing with us in-vivo data from the HIBISCUS cohort

T. Boutelier and H. Rebbah are with the Department of Research and Innovation, Olea Medical, 93 avenue des Sorbiers, 13600 La Ciotat, France (e-mail: timothe.boutelier@olea-medical.com; habib.rebbah@olea-medical.com).

K. Tse-Ve-Koon, P. Croisille and M. Viallon are with Univ Lyon, UJM-Saint-Etienne, INSA, Université Claude Bernard Lyon 1, CNRS UMR 5520, INSERM U1294, CREATIS, F-42023, SAINT-ETIENNE, France (e-mail: kevin.tsevekoon@creatis.univ-lyon1.fr;croisille@creatis.insa-lyon.fr; magalie.viallon@creatis.insa-lyon.fr)

for the independent estimate of the inversion efficiency [12], [14], which is difficult to acquire in a single breath hold. Besides, this simplification can introduce some bias in the estimation, which reduces the potential of the InSiL model [15].

We present a Bayesian estimation method of the InSiL parameters, that aims at dealing with the intrinsic limitations of the model in order to propose voxel wise estimation of every parameter without relying on model simplification. A Bayesian hierarchical model [16] is used with a multivariate Gaussian prior on the InSiL parameters. Prior parameters are estimated directly from the data, which makes the method free of pre-tuning of any parameters, hence particularly attractive in clinical practice. The resulting shrinkage effect pulls the estimates toward the group mean, thus making the proposed method less prone to outliers. Furthermore, the Bayesian framework naturally provides uncertainty measures of the parameter estimates, which is a valuable information for the quality check of the data and results.

The proposed estimation method is evaluated against classical MOLLI modeling and NLLS InSiL estimation using numerical simulations, physical phantoms, and illustrated in a test case of a patient with a chronic myocardial infarction (MI). The results show that the proposed Bayesian approach is able to give a more reliable T_1 estimation and with considerably reduced dependance of the estimates on the experimental conditions (HR, T_1, read-out sequence) compared to previous approaches.

II. Background

A. Classical MOLLI post processing

The MOLLI sequence for T_1 mapping [9] is based on 2 or 3 successive Look-Locker (LL) [17] acquisition cycles, separated by sufficient time laps that allow the longitudinal magnetization to recover between each LL cycle. Each cycle consists of an inversion pulse, followed by a succession of triggered bSSFP image readout at different TI synchronized with the heart cycle at end-diastole. Conveniently, each inversion pulse is applied at a slightly different instant in the heart cycle, so that different TI are sampled by each cycle. The original MOLLI sequence consists of 11 images using a 3(3)3(3)5 scheme, where three LL cycles are acquired and each cycle is composed of 3, 3, and 5 bSSFP readouts, respectively. Between each LL cycle, there is a resting period of 3 heartbeats to allow for the recovery of the longitudinal magnetization before the next inversion. This acquisition strategy allows to sample the full longitudinal magnetization recovery curve in one breath-hold of 17 heartbeats

The images acquired at different TI are then merged into one single dataset. The signal of each voxel at time TI after the inversion pulse is described by a 3 parameters monoexponential recovery model [18]:

$$S(TI) = A - B\exp\left(-TI/T_1^*\right) \tag{1}$$

where $T_1^* < T_1$ represents the apparent T_1 which is shortened by the influence of imaging RF pulses and imperfect inversion. The Look-Locker correction allows to convert the apparent T_1^* into T_1:

$$T_1 = T_1^*\left(\frac{B}{A} - 1\right)/\delta \tag{2}$$

where δ is the inversion factor that models the efficiency of the inversion pulse ($\delta \leq 1$).

T_1^*, A, and B parameters are estimated for each voxel using a NLLS algorithm that minimizes the sum of square errors (SSE) between the model and the data. However, (1) is valid only for phase sensitive inversion recovery (PSIR) acquisitions for which the sign of the signal is known, whereas in most clinical applications, only the magnitude is measured. Then one needs to take the absolute value of (1) for the model to be valid. Nonetheless, it is numerically more stable to use the original equation (1) and rely on a polarity estimation methods as described in [9]. For the remaining of the paper, T_1 estimation using this model and estimation method will be referred as the classical MOLLI method.

The classical MOLLI method has some limitations that makes it sensitive to tissue parameters T_1 and T_2, HR, sequence design, and imperfect inversion, which leads to T_1 underestimation [3], [19], [20]: First, longer T_1 or higher HR does not allow for the complete magnetization recovery at the end of each LL cycles, so that the subsequent cycles start with an increasing bias [13], [19], [21]. Second, the Look-Locker correction in (2) has been derived as an approximation for continuous fast low angle shot (FLASH) gradient echo readout with constant and short sampling time step [18]. In the MOLLI sequence, a bSSFP readout is used, and the time step is the time between two heartbeats of the patient, which is of the order of the T_1 and may be variable. This yields biases that are related to the tissue properties T_1 and T_2, bSSFP acquisition parameters, and the patient clinical condition [19]. Last, the classical MOLLI method does not allow to estimate the inversion efficiency, so it requires an independent measurement of this correction factor, that must be made prior to the MOLLI sequence.

Several sequence optimizations have been proposed to reduce the dependence of T_1 on those confounding factors [10], [21], but none succeeds to solve all the issues aforementioned [3], [22]. Modeling approaches seems a more promising alternative in this regard, as they propose to explicitly take into account some of those effects in the model of the MOLLI signal [12], [15], [23], [24].

B. InSiL model

The InSiL model [12] proposes a detailed simulation of the magnetization evolution during the MOLLI sequence, which is governed by 3 equations. First, the imperfect inversion pulse is modeled by a parameter δ which is assumed to be equal for each inversion pulse in the sequence. The magnetization immediately after an inversion is computed as:

$$M_{inv}^{+} = -\delta M_{inv}, \tag{3}$$

where M_{inv}^{+} is the magnetization following the inversion pulse, and M_{inv} is the magnetization immediately before the inversion. The longitudinal magnetization loss during the bSSFP

readout is modeled by an instantaneous loss, parametrized with a parameter C which is assumed to be constant for each readout:

$$M^+ = (1 - C)M, \tag{4}$$

where M^+ is the magnetization directly after the readout, and M before the readout. The longitudinal magnetization recovery between each readout is modeled by a classical monoexponential behavior:

$$M_k = M_0 + [M^+_{k-1} - M_0] \exp\left\{-\frac{(T_k - T_{k-1})}{T_1}\right\}, \tag{5}$$

where M_0 is the steady state magnetization, T_k denotes the successive times when either an inversion pulse is applied or the k-space center point of a single shot image is acquired during the MOLLI sequence. M_k and M^+_k are the longitudinal magnetization before and after either an inversion pulses or a single-shot acquisitions.

Such a design model explicitly handles HR variations, imperfect inversion and recovery of the magnetization, and magnetization loss during the readouts. The parameter δ models the imperfection of the inversion pulse. It is affected by the tissue T_1 and T_2 values [22], but also by the hardware quality, like B_1 inhomogeneities. Blood flow can also affect this parameter since uninverted spins can enter the acquired slice after the inversion pulse. This parameter is supposed to be bounded between 0 and 1. C parameter is mainly influenced by readout acquisition parameters (flip angle) and tissue magnetic properties. Indeed, short T_2 tissues are expected to have higher signal loss during the readout, which in turn yields higher values for this parameter. Its values are bounded between 0 and 1.

In [12], InSiL parameters (M_0, T_1 and C) are estimated for each voxel using a NLLS approach, by minimizing the sum of square error assuming that δ is known. [12] designed a "MOLLI+M_0" sequence inspired from [14] in order to estimate the inversion factor δ in-vivo. In [12], δ was measured on 4 healthy volunteers, then averaged to be used in the optimization problem.

III. Method

The Bayesian framework provides a method to update prior belief on model parameters as new data are measured. This is done using the Bayes' theorem, that describes how to combine *a priori* knowledge on the parameters and information provided by the data:

$$p(\Theta|D) = \frac{p(\Theta)p(D|\Theta)}{\int_\Theta p(\theta)p(D|\Theta)\,\mathrm{d}\theta} \tag{6}$$

where D stands for the experimental data, Θ is the set of parameters to be estimated, and θ is a particular parameter. $p(D|\Theta)$ is the likelihood, $p(\Theta)$ is the joint prior distribution, and $p(\Theta|D)$ is the joint posterior distribution, from which inference can be made on the parameters. The estimation problem casts now a problem of probability calculation. Hence, the solution of the problem lays into correctly addressing the likelihood and the prior distributions.

A. Likelihood

In this section, the MOLLI signal given by the InSiL model is parametrized as:

$$y_n = M_0 m_n(\Theta) + \epsilon_n, \tag{7}$$

where $m_n(\Theta)$ is the part of the signal that depends only on $\Theta = [T_1, C, \delta]$ at the n^{th} acquisition, and ϵ_n is an error term due to the noise. The noise is assumed to be independent and identically distributed, and we chose to model it by a zero-mean Normal distribution with variance σ_y^2. Hence the likelihood can be written as:

$$p(\mathbf{y}|\Theta, M_0, \sigma_y^2) = \left(2\pi\sigma_y^2\right)^{-N/2} \exp\left(-\frac{1}{2\sigma_y^2}(\mathbf{y} - M_0\mathbf{m})^T(\mathbf{y} - M_0\mathbf{m})\right), \tag{8}$$

where $\mathbf{y} = [y_1, \cdots, y_N]^t$ and $\mathbf{m} = [m_1, \cdots, m_N]^t$ are the vectors containing the N samples of the signal y_n and the corresponding model m_n respectively. M_0 and σ_y^2 are nuisance parameters, in the sense that they are required to build the model, but their knowledge is of no interest in this application. Hence, they can be marginalized to remove any explicit dependency on them, while retaining the influence of their estimation uncertainty on the other parameters of interest. This is done using the Bayes' theorem and the law of total probabilities by assigning an *a priori* distribution $p(M_0, \sigma_y^2)$. Hence, the marginal likelihood of the data is given by the integral over M_0 and σ_y^2:

$$p(\mathbf{y}|\Theta) = \int_0^\infty \left(\int_{-\infty}^\infty p(M_0, \sigma_y^2)p(\mathbf{y}|\Theta, M_0, \sigma_y^2)\,\mathrm{d}M_0\right)\,\mathrm{d}\sigma_y^2 \tag{9}$$

A conjugate Gaussian-Invers-Gamma g-prior [25] is used, that is defined as:

$$p(M_0, \sigma_y^2) = \mathcal{N}(M_0|0, \lambda^2\sigma_y^2/(\mathbf{m}^T\mathbf{m}))\mathcal{IG}(\sigma_y^2|\alpha, \beta), \tag{10}$$

where $\mathcal{N}()$ is the Gaussian distribution, and $\mathcal{IG}()$ is the Inverse-Gamma distribution. The first term is a zero-mean Gaussian distribution over M_0, whose variance is the noise-to-signal ratio $\sigma_y^2/(\mathbf{m}^t\mathbf{m})$, scaled by a factor λ^2. This distribution becomes very broad for large λ, which corresponds to a non-informative prior that ensures that M_0 will be influenced by the data rather than by the prior. Similarly, the Inverse-Gamma distribution on the noise variance σ_y^2 becomes non-informative when α and β are small. The prior was chosen because the marginalization can be done analytically and it can be parametrized so that it encodes a lack of prior information. In the limit $\lambda \gg 1$ and $\alpha, \beta \ll 1$, the marginalized likelihood is given by:

$$p(\mathbf{y}|\Theta) \propto \left[\mathbf{y}^T\mathbf{y} - \frac{(\mathbf{y}^T\mathbf{m})^2}{\mathbf{m}^T\mathbf{m}}\right]^{-N/2}, \tag{11}$$

where the dependance of the right-hand side of this equation on the InSiL parameters Θ is inside the $\mathbf{m}$ term. The proportionality constant depends on λ, α and β, but not on the InSiL parameters T_1, C or δ. Since the Markov Chain Monte Carlo (MCMC) algorithm used to make inference about the model parameters relies on the computation of ratio of

marginal likelihood evaluated at different model parameters value, this constant naturally cancels so its expression is not shown here.

B. Hierarchical prior

In order to complete the Bayesian model, a prior distribution on the model parameters must be attributed. A hierarchical prior is used, meaning that the assumption is made that Θ of each voxel in a given region of interest (ROI) are drawn from the same prior distribution. In order to ensure physical constraints on the model parameters ($0 < T_1$, $0 < C < 1$, $0 < \delta$), the prior is expressed on transformed parameters $t = \log(T_1)$, $c = \log(C/(C-1))$, and $d = \log(\delta)$, which map the domain of validity of each parameter on the entire real line.

1) 3 parameters hierarchical modeling: In a first implementation of the model, the prior is chosen as a multivariate Gaussian distribution on the three voxel wise transformed parameters (t, c, d):

$$p(\boldsymbol{\theta}_i|\boldsymbol{\mu}, \Sigma) = |2\pi\Sigma|^{-1/2} \exp\left(-\frac{1}{2}(\boldsymbol{\theta}_i - \boldsymbol{\mu})^T\Sigma^{-1}(\boldsymbol{\theta}_i - \boldsymbol{\mu})\right), \tag{12}$$

where $\boldsymbol{\theta}_i = [t_i, c_i, d_i]^T$ is the vector of transformed parameters for the voxel i, $\boldsymbol{\mu} = [\mu_t, \mu_c, \mu_d]^T$ is the mean of the distribution, and Σ is a 3×3 positive definite covariance matrix. The prior distribution describes the heterogeneity across the voxels taking into account any correlations between the parameters. Note that this prior is common for all the voxels that are analyzed, and that the hyper parameters $\boldsymbol{\mu}$ and Σ have to be estimated simultaneously with all voxels. A non-informative Jeffreys' prior [26] is used for the hyper-parameters on $\boldsymbol{\mu}$ and Σ:

$$p(\boldsymbol{\mu}, \Sigma) = |\Sigma|^{-1/2} \tag{13}$$

This model is later referred as the 3 parameters hierarchical Bayesian InSiL (HBI(3p)) model.

2) 2 parameters hierarchical modeling: In order to improve the robustness of the model, an alternative approach was tested, where T_1 and C are voxel wise parameters, and δ is set as a common parameter for all voxels. In that case, the hierarchical model applies to $\boldsymbol{\theta}_i = [t_i, c_i]^T$, with $\boldsymbol{\mu} = [\mu_t, \mu_c]^T$, and Σ is a 2×2 covariance matrix. The equations for the prior and hyper prior are the same as in the HBI(3p). To complete the model, a non informative uniform prior is used for d:

$$p(d) \sim 1 \tag{14}$$

This implementation with constant δ for every voxel is the Bayesian counterpart of the NLLS approach used in [12], with the additional feature that δ is estimated from the data and not fixed to an *a priori* value. In the remaining, this model is referred as the 2 parameters hierarchical Bayesian InSiL (HBI(2p)) model.

C. Posterior probability

The full posterior is computed applying the Bayes' theorem by combining the marginalized likelihood (11), the prior on the InSiL parameters (12), the hyper prior (13), and the prior on d in the case of the HBI(2p) model (14). The posterior for the HBI(3p) model is:

$$p(\boldsymbol{\theta}_{1:M}, \boldsymbol{\mu}, \Sigma|\mathbf{y}_{1:M}) \propto p(\boldsymbol{\mu}, \Sigma) \prod_{i=1}^{M} p(\mathbf{y}_i|\boldsymbol{\theta}_i) p(\boldsymbol{\theta}_i|\boldsymbol{\mu}, \Sigma), \tag{15}$$

where M is the number of voxels that are analyzed. The posterior distribution is over both the voxel-wise and the prior parameters, which are jointly inferred from the data. It implies that the estimation of any parameters of a particular voxel depends on all the voxels in the ROI, through their influence on the prior hyper-parameters, which is a characteristic feature of hierarchical models. A graphical representation of the Bayesian network underlying the hierarchical modeling used to do the parameter estimation with HBI(3p) is available in supplementary materials.

The estimation of a voxel-wise parameter is given by the expected value (mean) of its posterior distribution:

$$\widehat{t_i} = \int t_i p(\boldsymbol{\theta}_{1:M}, \boldsymbol{\mu}, \Sigma|\mathbf{y}_{1:M}) \, \mathrm{d}\boldsymbol{\theta}_{1:M} \, \mathrm{d}\boldsymbol{\mu} \, \mathrm{d}\Sigma \tag{16}$$

and similarly for c_i and d_i. Estimator of $\boldsymbol{\mu}$ or Σ can be derived in a similar manner to give heterogeneity or correlation measures over the voxels. Uncertainty on the estimators can be estimated by computing the variance of their posterior probability distribution:

$$\widehat{\sigma^2_{t_i}} = \int (t_i - \widehat{t_i})^2 p(\boldsymbol{\theta}_{1:M}, \boldsymbol{\mu}, \Sigma|\mathbf{y}_{1:M}) \, \mathrm{d}\boldsymbol{\theta}_{1:M} \, \mathrm{d}\boldsymbol{\mu} \, \mathrm{d}\Sigma \tag{17}$$

Additionally, the Bayesian framework offers the possibility to compute credible intervals and bets on those intervals from the posterior.

D. Markov Chain Monte Carlo

The estimation of any parameter of interest requires to compute integrals over a very large number of variables, which is analytically intractable. Furthermore, brute force computation of those integrals is also doomed by the curse of dimensionality. Here we rely on Markov Chain Monte Carlo (MCMC) method [27] to approximate those integrals. The principle of the MCMC method is to generate random samples of each parameter from a Markov chain, whose stationary distribution is the posterior distribution. After a certain burnin period, the chain will generate random samples that follow the desired posterior distribution. Eventually, any statistic of the posterior distribution can be computed from the Markov chain output by averaging the samples. For instance, the estimate and variance of t_i defined in (16) and (17) can be approximated by:

$$\widehat{t_i} \approx \frac{1}{N_s} \sum_{j=1}^{N_s} t_i^{(j)} \quad \text{and} \quad \widehat{\sigma^2_{t_i}} \approx \frac{1}{N_s} \sum_{j=1}^{N_s} (t_i^{(j)} - \widehat{t_i})^2 \tag{18}$$

The Markov chains were initiated from the T_1 and C parameters values estimated with the classical MOLLI approach and a numerical approximation valid for constant HR [28]. δ was initialized with random values uniformly sampled in the interval $[0.8; 1]$. The burnin period was chosen to 5000 iterations in order to ensure that the chain had converged for

every parameter. Further $N_s = 15000$ iterations were sampled to construct the Markov chain from which parameters and uncertainty estimation could be derived using (18). A detailed description of the algorithm can be found in the appendix in supplementary materials.

IV. Experiments

A. Numerical simulations

A numerical phantom was designed to benchmark the properties of the estimation methods for the InSiL and classical MOLLI model. The MOLLI signal was generated using the InSiL model for different sets of realistic parameter values (M_0, T_1, C, δ), and an additive Gaussian noise with standard deviation σ. The noise level was parametrized by the signal to noise ratio (SNR) that was defined as $SNR = M_0/\sigma$. M_0 was kept constant to 1 in all the phantom so the noise level was tuned via σ. The noise level was fixed to $SNR = 20$, which was found to be similar to what is observed in our in-vivo dataset. T_1 varied between 200 ms to 2000 ms with 200 ms step. C took its value between 0.1 and 0.3 with 0.05 step, and δ between 0.88 and 0.96 with 0.02 step. For each set of parameters, 100 signal curves were generated with different noise realizations.

In order to evaluate the robustness of the estimation methods to the MOLLI sequence scheme, the signal was sampled for the native and post-injection protocol at different TI. The same protocol as in the in vivo dataset was used: 5(3)3 and 4(1)3(1)2 for the native and post injection protocol respectively. Furthermore, different HR ranging from 40 bpm to 120 bpm were used to generate the data in order to evaluate the robustness of the method to the HR.

The simulated datasets were post processed with the classical MOLLI method, the NLLS method on all 4 InSil parameters (later referred as LSQ(4p)), the NLLS method on the 3 InSiL parameters with the inversion efficiency fixed *a priori* to the ground truth value of the phantom (later referred as LSQ(3p)), the HBI(3p) and HBI(2p) Bayesian models.

The estimation results were then compared to the ground truth values by computing the error in the T_1 estimation as $T_{1err} = 100 \times (E[T_{1est}] - T_{1gt})/T_{1gt}$ for each T_{1gt} ground truth value in the phantom, where $E[T_{1est}]$ is the average T_1 estimation in the phantom for a given T_{1gt}. Additionally, the dispersion in the estimation was computed as $T_{1sd} = 100 \times SD[T_{1est}]/E[T_{1est}]$, where $SD[T_{1est}]$ is the standard deviation of the T_1 estimation in the phantom for a given T_{1gt}. The variability of the estimation under different HR values was computed as $T_{1var} = 100 \times SD[\overline{T_1}]/E[\overline{T_1}]$, where $\overline{T_1}$ is the mean estimated T_1 for a given HR value, and $E(.)$ and $SD(.)$ indicate the mean and standard deviation computed over the different HR values. Similar statistics were computed for C and δ parameters.

B. Physical Phantom

An agarose gel-based phantom, using nickel chloride as the paramagnetic relaxation modifier, described in detail in [29], was scanned on a SIEMENS 3T MAGNETOM PRISMA clinical scanner using the product body array coil as anterior part and the corresponding elements of the spine coil as posterior part (18 channels in total) as used to explore cardiac patients. It contains nine differently doped agarose gel tube embedded in a gel/beads matrix in order to reduce B_1 inhomogeneities. Each tube corresponds to a specific couple of T_1/T_2, reported in [29]. The reference values of T_1 and T_2 of each vial are reported in [29], but we chose to measure our own reference values for T_1.

Reference T_1 values were measured using an inversion recovery spin echo sequence (TE = 6.5 ms, TR = 10000 ms, Flip Angle 90°) with 14 samples at TI=50, 100, 150, 200, 300, 450, 600, 800, 1000, 1500, 2500, 5000, 8000, and 9980 ms. The signal was fitted with a mono-exponential recovery model. The reference inversion efficiency δ was estimated with a modified MOLLI sequence [14], similar to what is described in [12]. The signal was then fitted with the InSiL model, with T_1 fixed to the reference value. Eventually, averaged values of T_1, and δ in circular regions of interest (ROI) of same size (5 cm^2) that were placed at the center of each tube were taken as reference values.

IR and MOLLI sequences were acquired using the same acquisition parameters (FoV 200 × 200 mm, voxel size 1.4/1.4/8 mm) and the phantom was not moved between experiments in order that the acquisition are perfectly registered, so the same ROIs could be used for all acquisitions. The temperature was controlled and monitored during all the experiment and found constant and equal to 22° C.

In order to evaluate the proposed Bayesian approach,various experimental scenarios were designed, by varying the MOLLI scheme, the rest period duration, the readout sequence, and the simulated ECG used to trigger the acquisitions. ECG with constant and variable HR values were simulated. The analysis of the mean HR of each MOLLI acquisition in our patient database revealed two different patient populations: one characterized by slow HR (mean: 55 bpm, standard deviation: 6 bpm) and the second characterized by faster HR (mean: 73 bpm, standard deviation: 9 bpm). Hence, HR were drawn from those two Gaussian distributions in order to generate realistic ECG with variable HR. Furthermore, the ECG of three patients from the database with the highest HR variation within the MOLLI acquisition were included.

A table summarizing all the experimental settings used in the study can be consulted in the supplementary materials. For each set of parameters, the acquisitions were repeated 5 times for each experimental setting. A time out of at least 10s was observed between two consecutive acquisitions.

The MOLLI data were analyzed with the same estimation methods as for the numerical phantom. For the LSQ(3p) method, the inversion efficiency δ of each tube was fixed to the reference value. Mean and standard deviation of the T_1 estimation within the same circular ROI as for the IR reference acquisition were computed. Similarly to the numerical analysis, the error, dispersion, and variability under different set of experimental conditions was evaluated, where the ground truth value T_{1gt} was replaced by the reference T_1 measured with the IR sequence.

C. In Vivo Data

In vivo sample patient case is from the HIBISCUS STEMI myocardial infarction clinical cohort (ClinicalTrials.gov Identifier: NCT03070496). Native and post injection T_1 maps acquired with 5(3)3 and 4(1)3(1)2 protocol schemes respectively were computed with the 5 same methods applied to the numerical and physical phantom. The extracellular volume [30] was computed as $ECV = (1-H_{ct})(R_{1myo}^{post} - R_{1myo}^{native})/(R_{1blood}^{post} - R_{1blood}^{native})$ where H_{ct} is the haematocrit and measured to 0.45 for the selected patient, and $R_1 = 1/\bar{T}_1$ where $\bar{T}_1$ is the average relaxation time of the myocardium or the blood, native or post injection respectively.

V. Results

A. Numerical Phantoms

Fig. 1 shows the error of the InSiL parameters estimation as a measure of the accuracy of the different methods on the phantom data at 60 bpm, with the native and post injection protocols. Fig. 2 shows the dispersion of the InSiL parameters estimation as a measure of the precision of the estimation methods for the same dataset.

1) T_1 estimation: Fig. 1 shows that classical MOLLI (orange circles) has a poor accuracy, since it systematically underestimates the true T_1, especially for the post injection protocol (4(1)3(1)2) for which the underestimation goes up to 30% for the longer T_1 . The results for the native protocol (5(3)3) are slightly better with an underestimation bounded between 5 % and 15 % depending on T_1. However, Fig. 2 shows that the precision of this method is excellent ($T_{1sd} \simeq 6$ %) for all T_1 values but for the shortest one in the phantom ($T_1 \leq 600$ ms).

Non linear least square fitting of all the InSiL parameter (LSQ(4p), light-blue diamonds) is by far the worst T_1 estimation method in term of accuracy (Fig.1) and precision (Fig. 2). On the opposite, fixing the inversion efficiency parameter to the true value (LSQ(3p), green squares) greatly improves the accuracy, with almost no error for all T_1. The dispersion of estimated T_1 values is around 7.5 % for the both protocols.

Hierarchical Bayesian modeling of the InSiL model gives very good results in term of accuracy, with an error that is slightly higher than LSQ(3p) with $|T_{1err}| < 2$ % for all T_1 and both protocols. The precision of the estimates is fairly the same for all T_1 values. It is better for HBI(2p) (dark blue upward triangle, $T_{1sd} \simeq 7.5$ %) than for HBI(3p) (yellow downward triangle, $T_{1sd} \simeq 9.5$ %).

2) C estimation: Fig. 1 shows that all estimation methods have a similar accuracy, with large estimation error depending on the C values. The same trend is observed for all methods and both acquisition protocols: small C are overestimated and the overestimation decreases with increasing C. For the classical MOLLI and Bayesian methods, the sign of the error eventually changes and estimated C becomes increasingly underestimated with increasing C. On the other hand, the error of the LSQ(3p) method seems to vanish when C is high.

Fig. 2 shows that the dispersion in the estimation of C is very large around 100 % for the non Bayesian methods (classical MOLLI, LSQ(4p), LSQ(3p)). On the opposite, HBI(3p) and HBI(2p) have a much lower dispersion, around $\sim 25\%$ for both methods and both protocols.

3) δ estimation: As δ is estimated only by LSQ(4p), HBI(3p) and HBI(2p) methods, only the results from those algorithms have been analyzed. Surprisingly, the estimation of δ by LSQ(4p) method is quite accurate, with an error of 1 % for the native protocol, and -4 % for the post injection protocol, in contrast to the other InSiL parameters estimated by this method (Fig. 1). However, the dispersion of the estimation is high, reaching more than 25 % for the native protocol.

The Bayesian method on the opposite shows a bias between -4 % and 4 %, with an overestimation of the small δ and an underestimation of the large δ. The average error of HBI(2p) is close to 0, meaning that the method was able to estimate accurately the average δ in the phantom. Estimation by HBI(3p) as a good precision, with a dispersion around 5 %. As δ is assumed constant for every voxel in the HBI(2p) method, the dispersion for this method is null. The results obtained with the Bayesian approaches are fairly independent on the acquisition protocol.

B. Physical Phantoms

1) Results averaged over all acquisition conditions: Fig. 3 shows a summary of each algorithm performance on the physical phantom averaged over all experimental conditions.

T_1 estimation with the MOLLI methods (orange circles) shows contrasted results. It has a poor accuracy, as it always underestimates T_1, especially at higher T_1 where the underestimation can reach 20 % (Fig. 3 top left). On the opposite, the precision of the method is excellent: Fig. 3 (top right) shows that the maximum dispersion is lower than 2.5 % for very short T_1, and it falls under 1 % for T_1 greater than ~ 400 ms. The variability under the different acquisition conditions varies between 5 % and 12 %, especially at longer T_1 (bottom of Fig. 3).

T_1 estimation with the InSiL model and the non linear estimation method LSQ(4p) (blue diamonds) gives the worst results, with the largest error, dispersion, and variability among all estimation methods (Fig. 3).

Fixing δ to its reference value as it is done with the LSQ(3p) method (green squares) considerably improves the results of the InSiL model. The average error on T_1 estimation is lower than 5 %, indicating a very good accuracy of the model. Furthermore, the method has a high precision, as indicated by a dispersion lower than 1 % for all T_1. Furthermore, the method is very robust to different acquisition conditions, as Fig. 3 indicates a variability below 5 % for short T_1, falling below 2 % for long T_1.

The Bayesian approach yields the best compromise between accuracy, precision, robustness, and dependence on the readout sequence. Indeed, HBI(3p) and HBI(2p) methods show the lowest average error, except for HBI(2p) at long T_1 where the T_1 is overestimated (Fig. 3). The precision of HBI(2p) is the best among all methods, as indicated by the lowest dispersion for every T_1. In comparison, the precision of the LSQ(3p) method is slightly degraded, with a dispersion reaching almost 1.7 %, which is a little bit worse than the

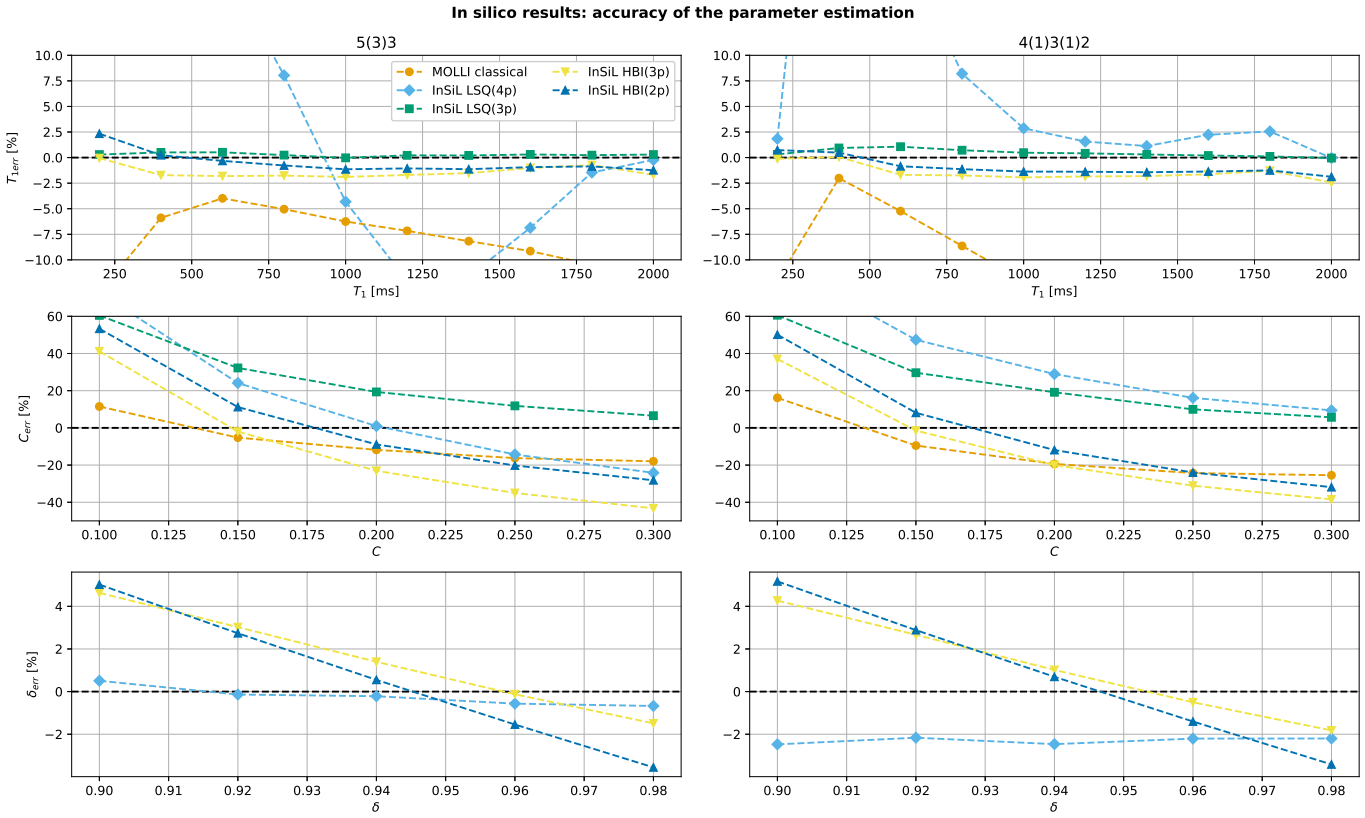

Fig. 1. Simulation results: error in the estimation of $\boldsymbol{T_1}$ (up), $\boldsymbol{C}$ (middle) and $\boldsymbol{\delta}$ (down) for the 5(5)3 (left) and the 4(1)3(1)2(1) (right) protocols with the numerical phantom data at **60** bpm. Classical MOLLI results are indicated by orange circles, LSQ(4p) with light-blue diamonds, LSQ(3p) with green squares, HBI(3p) with downward yellow triangles, and HBI(2p) with upward dark blue triangles. Since $\boldsymbol{\delta}$ is not estimated but fixed a priori with classical MOLLI and LSQ(3p) methods, $\boldsymbol{\delta_{err}}$ is not shown for those methods.

precision of the classical MOLLI or the non linear InSiL LSQ(3p). Still, it is far better than LSQ(4p). Those results are confirmed when looking at the robustness of the T_1 estimation to the HR variation and acquisition scheme (see supplementary materials.)

C. In Vivo Data

Fig. 4 shows that LSQ(4p) estimation method produces images with very poor quality, unsuitable for clinical analysis. On the opposite, the Bayesian estimation method HBI(3p) allows to have an image qualitatively equivalent to the the one obtained with the MOLLI classical estimation method. The quantitative comparison between the two methods for the post injection acquisition, shows that classical MOLLI underestimates T_1 compared to HBI(3p) in the healthy myocardium ($\sim 15\%$), in the lesion ($\sim 20\%$) and in the left ventricle ($\sim 10\%$). The underestimation is lower for the native acquisition with ($\sim 10\%$) in the myocardium, and ($\sim 5\%$) in the left ventricle (see supplementary material). However, this underestimation has no significant effect on the ECV computation for this patient. The uncertainty on the ECV estimation is similar for every estimation methods but for LSQ(4p) which is much higher than the others (see supplementary materials).

VI. Discussion

The simulations, physical phantom acquisition, and in vivo data used in this work show that the classical 3 parameters mono-exponential modeling of the MOLLI sequence generates underestimated T_1 values. Furthermore, estimated T_1 are sensitive to confounding experimental factors such as sequence design, sequence readout, and HR variations. Those findings are in agreement with what has already been reported in previous studies evaluating the accuracy of cardiac T_1 mapping measured with the MOLLI sequence [3], [13], [19], [20].

The InSiL model was introduced in an attempt to correct those defects and enable a more accurate estimation of T_1 [12]. Both our in silico and in vitro results show that the model is able to generate accurate and precise T_1 estimation, on the condition that the other parameters introduced by this model are well estimated. Hence, the estimation of the voxel wise parameters using a classical non linear least square optimization method (LSQ(4p)) yields strongly biased and dispersed estimated T_1 values, as can be seen on figures 1 to 4. T_1 maps generated with this approach displays image of poor quality that have no clinical use (see Fig. 4, center). On the opposite, setting the inversion efficiency δ to an *a priori* fixed value (LSQ(3p)), allows to recover precise T_1 estimation. In our numerical and physical phantom experiments, δ was set to its true known value. This corresponds to an ideal situation, that cannot be met in clinical condition. This approach was

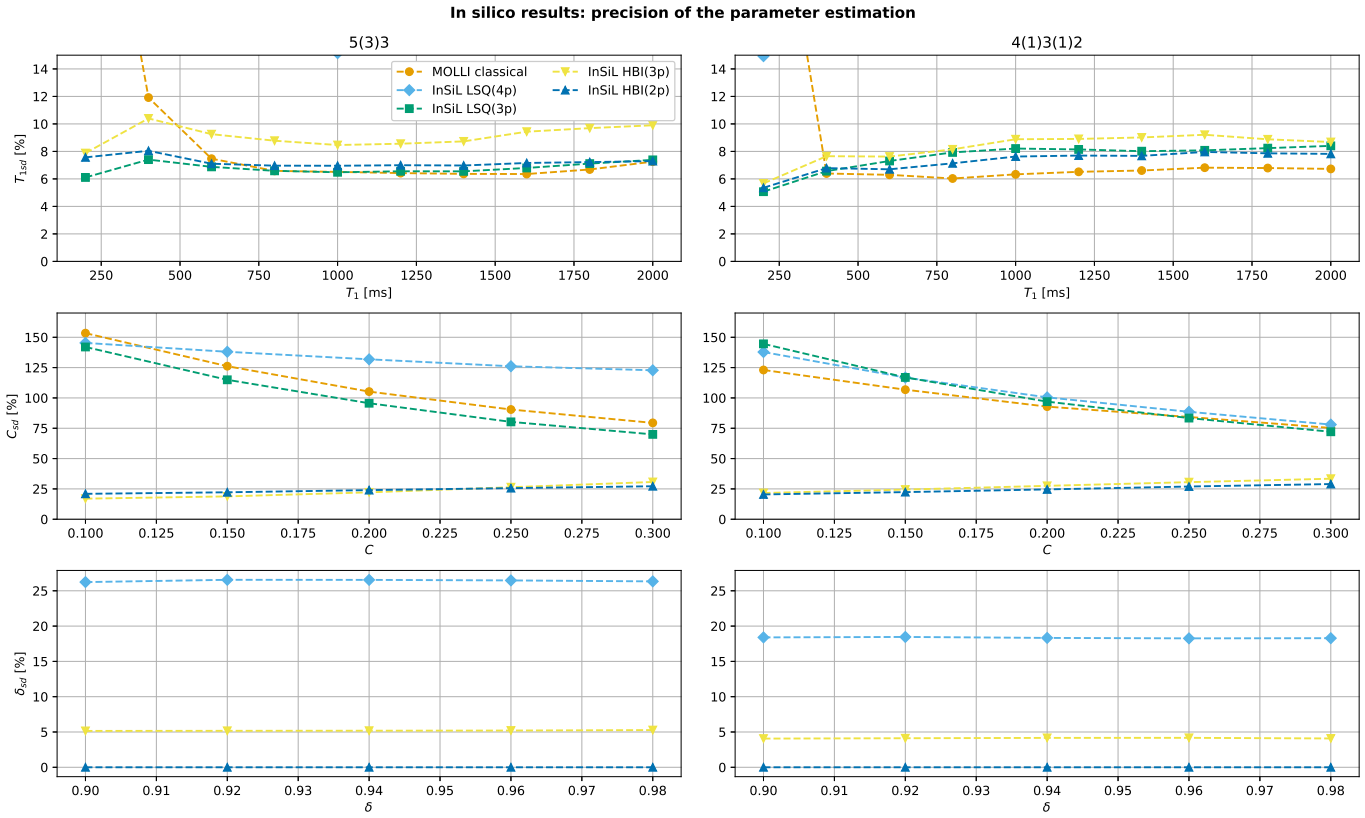

Fig. 2. Simulation results: dispersion of T_1 (up), C (middle) and δ (down) estimation for the 5(5)3 (left) and the 4(1)3(1)2(1) (right) protocols with the numerical phantom data at 60 bpm. Colors and markers are the same as in Fig. 1

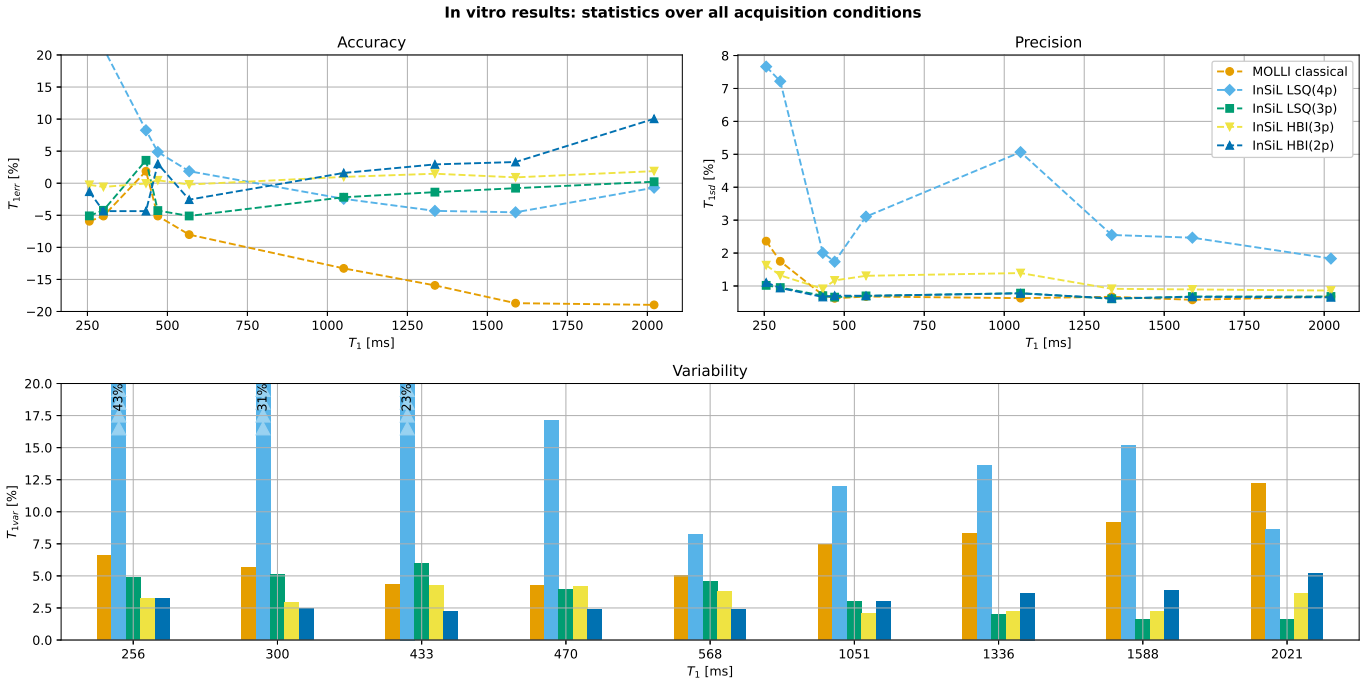

Fig. 3. In-vitro results: T_1 averaged over all acquisition conditions: percentage of error (top left), dispersion (top right),and variability (bottom) under those experimental conditions. Colors and markers are the same as in Fig. 1.

proposed in [12], [13], using an additional sequence [14] to independently estimate the inversion efficiency parameter, and averaging it to a single value used in the model for all voxels. Hence, classical non linear least square approach requires bold assumption on some parameters, that are hardly practical in clinical routine.

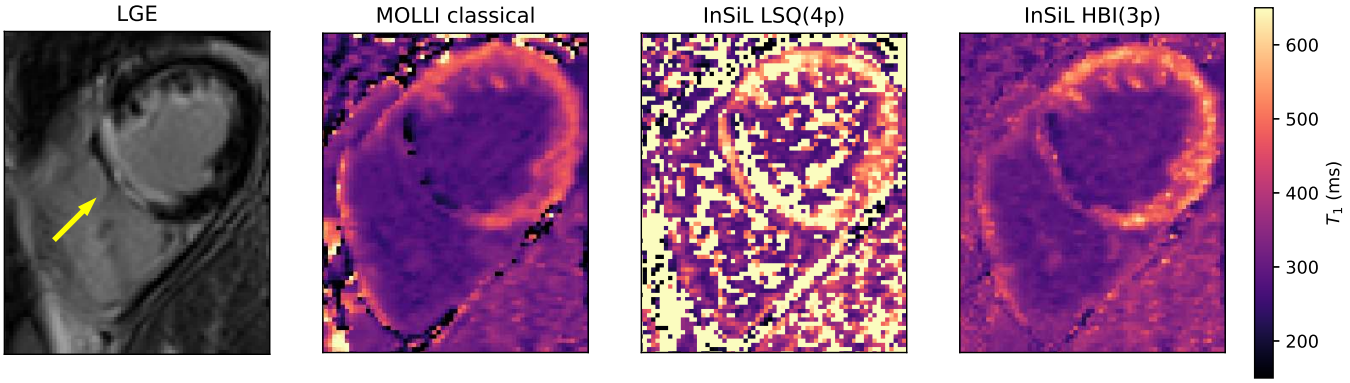

Fig. 4. In vivo results in a 62 years old male patient with a chronic myocardial infarction, acquired after gadolinium injection with a 4(1)3(1)2 MOLLI sequence. From left to right: Late Gadolinium Enhancement image (the yellow arrow indicates the lesion), post injection $\boldsymbol{T_1}$ computed with the MOLLI model, LSQ(4p), and HBI(3P).

The proposed hierarchical Bayesian model is an alternative approach estimation method of the InSiL parameters. The numerical and in vitro phantom experiments show that this approach has similar T_1 precision and accuracy compared to the LSQ(3p) classical approach. However, it has the advantage of not requiring to fix the inversion efficiency parameter *a priori*, which is a strong *a priori* that cannot be made in clinical practice.

This new estimation method is the first one that allows to reliably estimate the inversion efficiency δ and the readout losses C on a voxel wise basis from the MOLLI data only. This is a direct consequence of the shrinkage effect of the multivariate Gaussian prior on the model parameters, that has the effect of pulling outliers estimated values toward the group mean. This effect can be clearly observed on Fig. 1 and 2: smaller C (center row) and δ (bottom row) are overestimated, while higher values are underestimated. The dispersion on the estimation is much lower compared to what classical method can do. This indicates that the multivariate Gaussian prior was estimated to be quite informative for those parameters (i.e. with a small variance), which introduces a slight bias in those parameters estimation. However, this has the huge benefit of stabilizing the estimation, which in turn benefits to the T_1 estimation.

Interestingly, simulations show that the shrinkage prior erases almost completely the variability of δ in HBI(3p), by setting it to an almost constant values which is equal to the average δ of all voxels in the ROI. This means that the HBI(3p) model can be reliably simplified by the HBI(2p) model where δ is set to a constant value for all voxels.

It is expected that the results of the hierarchical Bayesian method might depend on the choice of the ROI since it is what constrains the prior. A ROI with heterogeneous tissues, which have a wide range of T1 values, will likely yield results that will be biased toward the mean of the ROI. This would produce a bias where low T_1 values would be overestimated and high T_1 values would be underestimated. On the opposite, we expect optimal results for ROI with homogeneous tissue type. However, no strong under- or overestimation of the T_1 parameters was observed with the numerical or physical phantom data. This indicates that the shrinkage effect of the hierarchical model did not introduce bias in the T_1 estimation, even when a wide range of T_1 values are represented in the data, as it is the case in the simulations and in vitro experiments.

It is worth noting that when the HR is constant during the acquisition, all methods give the same results. This is due to the fact that the InSiL model is equivalent to the classical 3 parameters MOLLI model when HR is constant [28]. The fact that a 4 parameters model coincides with a 3 parameters model under some regular acquisition conditions shows that the InSiL is a degenerate model, which might be the root cause of the instability of the classical estimation method. The additional constraints on the parameters brought by the Bayesian approach allows to partially solve this problem. In that case, the Bayesian model naturally converges toward a situation where the inversion efficiency is constant.

The Bayesian model is built with the assumption that the noise follows a Gaussian distribution, whereas it has a Rician distribution [31]. Taking this into account in the model would be straightforward, as it would impact the likelihood of the data only (Eq. 8). However, replacing the Gaussian distribution by a Rician one would make some analytical calculation intractable like the marginalization of the initial magnetization and the noise standard deviation to obtain the marginal likelihood (Eq: 11). Hence those parameters would need to added to the MCMC chains, which would increase the computation time. Furthermore, compared to the Gaussian distribution, the Rician distribution is much more computationally expensive to estimate or sample, which would increase even more the computation time of the MCMC samples generation. For that reason we chose to simplify the model using a Gaussian distribution. We checked that this hypothesis had no effect on the parameter estimation by comparing the estimation on numerical phantom generated using Gaussian and Rician noise. No significant differences were found, showing that the noise distribution had no impact on the estimation.

VII. Conclusion

In this work, a hierarchical Bayesian modeling was proposed to estimate the voxel wise parameters of the InSiL

model from MOLLI acquisition. Contrary to previous proposed approaches based on non linear least square methods, all the model parameters are estimated without fixing some of them to *a priori* values. The parameters of the multivariate Gaussian prior used in the Bayesian model are estimated directly from the data, together with the model parameters. This makes the method free of tuning parameters, hence more objective. Numerical simulation, physical phantoms, and clinical data show that T_1 estimation uncertainty is considerably reduced thanks to the shrinkage effect of the priors, and falls in the range of what is obtained with the classical MOLLI estimation method. Hence, this estimation method allows for the first time to exploit the full potential of the InSiL model in clinical practice, and to get T_1 estimates that are more accurate, and less sensitive to confounding factors such as noise level, tissue properties, HR variability, sequence design and readout sequence. Despite better accuracy and precision, in depth clinical studies are needed to evaluate the added value of the InSiL model for the patient.

REFERENCES

[1] F. Bloch, "Nuclear Induction," *Phys. Rev.*, vol. 70, no. 7-8, pp. 460–474, oct 1946.

[2] H. L. Margaret Cheng, N. Stikov, N. R. Ghugre, and G. A. Wright, "Practical medical applications of quantitative MR relaxometry," *J. Magn. Reson. Imaging*, vol. 36, no. 4, pp. 805–824, 2012.

[3] S. K. Piechnik and M. Jerosch-Herold, "Myocardial T1 mapping and extracellular volume quantification: an overview of technical and biological confounders," *Int. J. Cardiovasc. Imaging*, vol. 34, no. 1, pp. 3–14, 2018.

[4] D. R. Messroghli, T. Niendorf, J. Schulz-Menger, R. Dietz, and M. G. Friedrich, "T1 Mapping in Patients with Acute Myocardial Infarction," *J. Cardiovasc. Magn. Reson.*, vol. 5, no. 2, pp. 353–359, 2003.

[5] M. Ugander, P. S. Bagi, A. J. Oki, B. Chen, L.-Y. Hsu, A. H. Aletras, S. Shah, A. Greiser, P. Kellman, and A. E. Arai, "Myocardial Edema as Detected by Pre-Contrast T1 and T2 CMR Delineates Area at Risk Associated With Acute Myocardial Infarction," *JACC Cardiovasc. Imaging*, vol. 5, no. 6, pp. 596–603, jun 2012.

[6] M. Fontana, S. K. White, S. M. Banypersad, D. M. Sado, V. Maestrini, A. S. Flett, S. K. Piechnik, S. Neubauer, N. Roberts, and J. C. Moon, "Comparison of T1 mapping techniques for ECV quantification. Histological validation and reproducibility of ShMOLLI versus multibreathhold T1 quantification equilibrium contrast CMR," *J. Cardiovasc. Magn. Reson.*, vol. 14, no. 1, p. 1, 2012.

[7] P. Kellman, J. R. Wilson, H. Xue, M. Ugander, and A. E. Arai, "Extracellular volume fraction mapping in the myocardium, part 1: Evaluation of an automated method," *J. Cardiovasc. Magn. Reson.*, vol. 14, no. 1, pp. 1–11, 2012.

[8] E. Kehr, M. Sono, S. S. Chugh, and M. Jerosch-Herold, "Gadolinium-enhanced magnetic resonance imaging for detection and quantification of fibrosis in human myocardium in vitro," *Int. J. Cardiovasc. Imaging*, vol. 24, no. 1, pp. 61–68, dec 2007.

[9] D. R. Messroghli, A. Radjenovic, S. Kozerke, D. M. Higgins, M. U. Sivananthan, and J. P. Ridgway, "Modified look-locker inversion recovery (MOLLI) for high-resolution T 1 mapping of the heart," *Magn. Reson. Med.*, vol. 52, no. 1, pp. 141–146, 2004.

[10] K. Chow, J. A. Flewitt, J. D. Green, J. J. Pagano, M. G. Friedrich, and R. B. Thompson, "Saturation recovery single-shot acquisition (SASHA) for myocardial T 1 mapping," *Magn. Reson. Med.*, vol. 71, no. 6, pp. 2082–2095, 2014.

[11] S. Weingärtner, M. Akcakaya, S. Berg, K. V. Kissinger, W. J. Manning, and R. Nezafat, "Heart-rate independent myocardial T1-mapping using combined saturation and inversion preparation pulses," *J. Cardiovasc. Magn. Reson.*, vol. 15, no. S1, p. P46, 2013.

[12] J. Shao, K. L. Nguyen, Y. Natsuaki, B. Spottiswoode, and P. Hu, "Instantaneous signal loss simulation (InSiL): An improved algorithm for myocardial T1mapping using the MOLLI sequence," *J. Magn. Reson. Imaging*, vol. 41, no. 3, pp. 721–729, 2015.

[13] J. Shao, D. Liu, K. Sung, K. L. Nguyen, and P. Hu, "Accuracy, precision, and reproducibility of myocardial T1 mapping: A comparison of four T1 estimation algorithms for modified look-locker inversion recovery (MOLLI)," *Magn. Reson. Med.*, vol. 78, no. 5, pp. 1746–1756, 2017.

[14] C. T. Rodgers, S. K. Piechnik, L. J. DelaBarre, P.-F. Van de Moortele, C. J. Snyder, S. Neubauer, M. D. Robson, and J. T. Vaughan, "Inversion recovery at 7 T in the human myocardium: Measurement of T 1 , inversion efficiency and B 1 +," *Magn. Reson. Med.*, vol. 70, no. 4, pp. 1038–1046, oct 2013.

[15] J. Shao, Z. Zhou, K. Nguyen, J. P. Finn, and P. Hu, "Accurate, precise, simultaneous myocardial T1 and T2 mapping using a radial sequence with inversion recovery and T2 preparation," *NMR Biomed.*, no. July, pp. 1–12, 2019.

[16] A. Gelman and J. Hill, *Data Analysis Using Regression and Multilevel/Hierarchical Models*. Cambridge: Cambridge University Press, 2006.

[17] D. C. Look and D. R. Locker, "Time saving in measurement of NMR and EPR relaxation times," *Rev. Sci. Instrum.*, vol. 41, no. 2, pp. 250–251, 1970.

[18] R. Deichmann and A. Haase, "Quantification of T1values by SNAPSHOT-FLASH NMR imaging," *J. Magn. Reson.*, vol. 96, no. 3, pp. 608–612, 1992.

[19] G. S. Slavin, "On the use of the "look-locker correction" for calculating T1 values from MOLLI," *J. Cardiovasc. Magn. Reson.*, vol. 16, no. S1, pp. 1–2, 2014.

[20] P. Kellman and M. S. Hansen, "T1-mapping in the heart: accuracy and precision," *J. Cardiovasc. Magn. Reson.*, vol. 16, no. 1, p. 2, dec 2014.

[21] S. K. Piechnik, V. M. Ferreira, E. Dall'Armellina, L. E. Cochlin, A. Greiser, S. Neubauer, and M. D. Robson, "Shortened Modified Look-Locker Inversion recovery (ShMOLLI) for clinical myocardial T1-mapping at 1.5 and 3 T within a 9 heartbeat breathhold," *J. Cardiovasc. Magn. Reson.*, vol. 12, no. 1, p. 69, 2010.

[22] P. Kellman, D. A. Herzka, and M. S. Hansen, "Adiabatic inversion pulses for myocardial T1 mapping," *Magn. Reson. Med.*, vol. 71, no. 4, pp. 1428–1434, apr 2014.

[23] J. Shao, S. Rapacchi, K. L. Nguyen, and P. Hu, "Myocardial T1 mapping at 3.0 tesla using an inversion recovery spoiled gradient echo readout and bloch equation simulation with slice profile correction (BLESSPC) T1 estimation algorithm," *J. Magn. Reson. Imaging*, vol. 43, no. 2, pp. 414–425, 2016.

[24] H. Rebbah, T. Galas, G. Soulat, N. Kachenoura, A. Menini, C. A. Cuenod, and E. Mousseaux, "Temporal registration: a new approach to manage the incomplete recovery of the longitudinal magnetization in the Modified Look-Locker Inversion Recovery sequence (MOLLI) for T1 mapping of the heart," *Magn. Reson. Mater. Physics, Biol. Med.*, jan 2020.

[25] A. Zellner, "On Assessing Prior Distributions and Bayesian Regression Analysis with g Prior Distributions," in *Bayesian Inference Decis. Tech. Essays Honor Bruno Finetti*, Elsevier, Ed., New York, 1986, pp. 233–243.

[26] H. Jeffreys, "An invariant form for the prior probability in estimation problems," *Proc. R. Soc. London. Ser. A. Math. Phys. Sci.*, vol. 186, no. 1007, pp. 453–461, sep 1946.

[27] N. Metropolis, A. W. Rosenbluth, M. N. Rosenbluth, A. H. Teller, and E. Teller, "Equation of state calculations by fast computing machines," *J. Chem. Phys.*, vol. 21, no. 6, pp. 1087–1092, 1953.

[28] H. Rebbah, "Quantification et optimisation de l'imagerie par résonnance magnétique de la perfusion cardiaque," Ph.D. dissertation, Paris Descartes, 2019.

[29] G. Captur, P. Gatehouse, K. E. Keenan, F. G. Heslinga, R. Bruehl, M. Prothmann, M. J. Graves, R. J. Eames, C. Torlasco, G. Benedetti, J. Donovan, B. Ittermann, R. Boubertakh, A. Bathgate, C. Royet, W. Pang, R. Nezafat, M. Salerno, P. Kellman, and J. C. Moon, "A medical device-grade T1 and ECV phantom for global T1 mapping quality assurance - the T1 Mapping and ECV Standardization in cardiovascular magnetic resonance (T1MES) program," *J. Cardiovasc. Magn. Reson.*, vol. 18, no. 1, pp. 1–20, 2016.

[30] P. Haaf, P. Garg, D. R. Messroghli, D. A. Broadbent, J. P. Greenwood, and S. Plein, "Cardiac T1 Mapping and Extracellular Volume (ECV) in clinical practice: A comprehensive review," *J. Cardiovasc. Magn. Reson.*, vol. 18, no. 1, pp. 1–12, 2016.

[31] H. Gudbjartsson and S. Patz, "The Rician distribution of noisy MRI data." *Magn. Reson. Med.*, vol. 34, no. 6, pp. 910–4, dec 1995.